MITSUBISHI ELECTRIC RESEARCH LABORATORIES
https://www.merl.com

Multi-pass Extended Kalman Smoother with Partially-known Constraints for Estimation of Vapor Compression Cycles

Deshpande, Vedang M.; Laughman, Christopher R.

TR2023-079 July 04, 2023

Abstract

State and parameter estimation methodologies have the potential to make a significant impact in the development of broad array of capabilities for widely-used vapor compression cycles, including advanced controls, performance monitoring, data-driven modeling, and deployment of digital twin technologies. However, the nonlinearity and numerical stiffness of large physics-based models of these systems pose challenges for the practical implementation of estimators that must also satisfy the physical state constraints. We present a three-pass fixed-interval smoothing method developed in the extended Kalman estimation formalism that incorporates linear inequality and partially-known nonlinear equality constraints defined in terms of unknown parameters of the system. The smoothing method is demonstrated to have high estimation accuracy during joint state and parameter estimation of the cycle model representing a realistic system that is implemented in Julia language leveraging automatic differentiation capabilities.

World Congress of the International Federation of Automatic Control (IFAC) 2023

Mitsubishi Electric Research Laboratories, Inc.
201 Broadway, Cambridge, Massachusetts 02139

Multi-pass Extended Kalman Smoother with Partially-known Constraints for Estimation of Vapor Compression Cycles

Vedang M. Deshpande[†] **Christopher R. Laughman**

Mitsubishi Electric Research Laboratories, Cambridge, MA 02139 USA
[†]*Corresponding author.* ✉ {*deshpande,laughman*}*@merl.com*

Abstract: State and parameter estimation methodologies have the potential to make a significant impact in the development of broad array of capabilities for widely-used vapor compression cycles, including advanced controls, performance monitoring, data-driven modeling, and deployment of digital twin technologies. However, the nonlinearity and numerical stiffness of large physics-based models of these systems pose challenges for the practical implementation of estimators that must also satisfy the physical state constraints. We present a three-pass fixed-interval smoothing method developed in the extended Kalman estimation formalism that incorporates linear inequality and partially-known nonlinear equality constraints defined in terms of unknown parameters of the system. The smoothing method is demonstrated to have high estimation accuracy during joint state and parameter estimation of the cycle model representing a realistic system that is implemented in Julia language leveraging automatic differentiation capabilities.

Keywords: Constrained estimation, Kalman filtering and smoothing, nonlinear state and parameter estimation, vapor compression cycle, HVAC

1. INTRODUCTION

Vapor compression cycles are used in a broad range of applications because they are a practical and cost-efficient system for heat transfer over a wide range of temperatures. Although they are cleaner in operation than the conventional fossil fuel-based heating systems, they raise valid environmental concerns as noted in a report by IEA (2018), because they consume about 10% of total electricity produced worldwide, and use working fluids whose global warming potential is often hundreds of times higher than carbon dioxide. Therefore, technologies that could further improve the overall performance of vapor compression systems deserve dedicated research efforts.

Estimation methods could prove to be an important tool in system identification, data-driven modeling efforts, and a range of control technologies employed in vapor compression cycles. Commercially sold systems have limited sensor availability due to cost-sensitive nature of these consumer equipment, thus making the state estimation methods crucial for estimating unmeasured quantities on which future control architectures and performance may depend. Robust parameter estimation methods may also facilitate fault diagnostics for the early identification of performance degradation because many system parameters, such as the refrigerant mass and heat transfer coefficients, may change over the equipment lifetime and cause significant energy waste. Moreover, accurate state and parameter estimation and calibration tools are central to the advancement and deployment of data-driven modeling and digital twin technologies for these systems, particularly in heating, ventilation, and air conditioning (HVAC) applications, see Vering et al. (2021); Bortoff and Laughman (2022); Chinchilla et al. (2022).

Previous works by Bortoff et al. (2019) and Krupa et al. (2019) have demonstrated the use of state estimation methods such as Kalman filter for designing, respectively, a robust model predictive controller (MPC) for a reduced order model and a linear MPC for nonlinear model of a multi-terminal vapor-compression cycle. Since heat exchangers (HEXs) dominate the overall dynamics of the vapor compression systems, they have received special attention in component level state estimation scenarios. For example, Cheng et al. (2005) developed a nonlinear observer for a reduced-order model of a HEX to accurately predict evaporating temperature and two-phase length for an experimental system, and more recently, Ghousein and Witrant (2019) developed a boundary observer for a concentric CO_2 HEX using Lyapunov analysis.

While the previous works have leveraged relatively low-order component and system models for efficient state estimation, more complex cycles that are in use today could benefit from these estimation methods in a broad range of applications mentioned earlier. However, implementation of classical estimation methods pose distinct challenges when used with physics-based behavioral models of larger complex systems. Heat and fluid flow in the HEXs used in these systems is governed by nonlinear partial differential equations (PDEs) that relate the conjugate heat transfer to the refrigerant dynamics, which is nonlinear and has discontinuous derivatives at the liquid and vapor saturation curves. While these PDEs can be discretized using finite volume representations of HEXs, it results in large sets of

index-1 nonlinear differential algebraic equations (DAEs) which are numerically stiff, have hundreds of state variables, and typically require specialized numerical solvers for integration.

In addition to these computational challenges, estimates obtained from classical estimation methods may not necessarily satisfy the state constraints imposed by the governing physical laws leading to failure of physics-based computational models which are often designed under the assumption that they operate in valid regions where such constraints are satisfied. In an effort to address these concerns, Deshpande et al. (2022) recently presented estimation methods in a fixed-interval smoothing context that explicitly enforce physics-based linear inequality constraints during the estimation process. These constrained smoothing methods were developed for cycle models without parametric uncertainties in both extended and ensemble Kalman formulations and the curse of growing dimensionality in the ensemble Kalman smoother was circumvented using a reformulation in the covariance range which makes the problem size equal to a constant ensemble size.

The present work is focused on the development of a nonlinear joint state and parameter estimation method that can leverage partially-known constraints in terms of unknown parameters of the system for better estimation accuracy. The method is formulated as a three-stage smoother in an extended Kalman framework which benefits from the computational capabilities of Julia [1] language ecosystem.

This paper's contributions, which are summarized below, lie at the domain intersection of theory and technological implementation.

- We present a fixed-interval smoother formulated in an extended Kalman formalism that incorporates linear inequality and partially-known nonlinear equality constraints defined in terms of unknown parameters of the system.
- We demonstrate a nonlinear joint state and parameter estimation framework for vapor compression cycles facilitated by automatic differentiation (AD) capable models developed in Julia.

In Section 2, we briefly discuss the cycle model and its implementation in Julia. The theoretical development of the constrained three-stage smoother is described in Section 3. Results demonstrating the performance of the smoother are presented in Section 4, followed by a brief summary of the work and potential future research directions in Section 5.

2. AUTOMATIC DIFFERENTIABLE CYCLE MODEL

Fig. 1 shows a schematic of a vapor compression cycle capable of varying the heating or cooling capacity delivered to an occupied space. It consists of a variable-position expansion device, a variable-speed compressor, and two refrigerant-to-air HEXs (condenser and evaporator) with variable speed fans. This system transfers thermal energy from the air passing through the evaporating HEX to the air passing through the condensing HEX via the refrigerant flowing through the system.

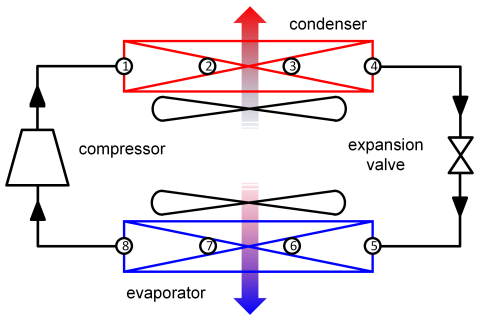

Fig. 1. Schematic diagram of a vapor compression cycle

While algebraic models were used for the compressor and expansion, the HEX models which dominate the overall dynamics, were constructed from finite volume discretizations. The HEX models consist of an interconnected set of models that describe the one-dimensional refrigerant pipeflow, the thermal behavior of the tube wall, and the flow of air across the heat exchanger, forming an index-1 system of DAEs.

The pipe model for the refrigerant enforces the following equations for conservation of mass, momentum, and energy,

$$\begin{aligned} \frac{\partial(\rho A)}{\partial t} + \frac{\partial(\rho A v)}{\partial x} &= 0 \\ \frac{\partial(\rho v A)}{\partial t} + \frac{\partial(\rho v^2 A)}{\partial x} &= -A\frac{\partial P}{\partial x} - F_f \\ \frac{\partial(\rho u A)}{\partial t} + \frac{\partial(\rho v h A)}{\partial x} &= vA\frac{\partial P}{\partial x} + vF_f + \frac{\partial Q}{\partial x} \end{aligned} \tag{1}$$

where ρ is the density, A is the cross-sectional area of the flow, v is the velocity, P is the pressure, F_f is the frictional pressure drop, u is the specific internal energy, h is the specific enthalpy, and Q is the heat flow rate into or out of the fluid. These equations use a spline-based representation of the thermodynamic refrigerant properties developed by Laughman and Qiao (2021). These equations can be adapted to a finite control volume discretization of the refrigerant pipe into an arbitrary number of volumes by using a staggered-grid approach. Further details about the models of HEX, compressor, and expansion valve are available in Qiao et al. (2015).

The cycle model is implemented using the Julia package `ModelingToolkit.jl` developed by Ma et al. (2021). This package uses a symbolic computational algebra framework that enables the construction of large acausal system models from smaller component models and generates imperative Julia code that can be used with other computational tools, including AD. This facilitates efficient Jacobian computations of the complete cycle dynamics with respect to both state variables and parameters; a functionality vital for the extended Kalman formalism.

For the purpose of this study, we consider a cycle model obtained by discretizing both HEXs into 4 volumes each which resulted in a set of 278 index-1 DAEs, which in turn was reduced to 24-dimensional nonlinear ODE using the index reduction algorithm by Pantelides (1988). The ODEs have the following form

[1] `https://julialang.org/`

$$\dot{\boldsymbol{x}}(t) = \boldsymbol{f}(\boldsymbol{x}(t), \boldsymbol{u}(t), \boldsymbol{\phi}), \tag{2}$$

where $\boldsymbol{x}$ is the state vector, $\boldsymbol{u}$ is the vector of known time-varying control inputs and system conditions (compressor speed, valve position, ambient temperatures, etc.), and $\boldsymbol{\phi}$ is the vector of time-invariant system parameters (geometric dimensions of pipes, material properties, etc.)

The finite volumes are numbered 1 through 8 in the direction of refrigerant flow, as shown in Fig. 1. The state vector $\boldsymbol{x}$ after index reduction is an augmented vector of pressures (P_i), specific enthalpies (h_i), and pipe wall temperatures (θ_i) of all finite control volumes indexed by the subscript $i = 1, \cdots, 8$. Therefore, the state vector $\boldsymbol{x} \in \mathbb{R}^{24}$ is defined as

$$\boldsymbol{x} \triangleq \left[P_1 \ h_1 \ \theta_1 \ P_2 \ h_2 \ \theta_2 \ \cdots \ P_8 \ h_8 \ \theta_8\right]^\top. \tag{3}$$

A temporally discretized model is obtained from (2) by

$$\boldsymbol{x}_{k+1} = \boldsymbol{x}_k + \int_{t_k}^{t_{k+1}} \boldsymbol{f}(\boldsymbol{x}(t), \boldsymbol{u}(t), \boldsymbol{\phi}) dt, \tag{4}$$

where $\boldsymbol{x}_k \triangleq \boldsymbol{x}(t_k)$.

In practice, the system parameters $\boldsymbol{\phi}$ are not exactly known and must be estimated or calibrated from the available data. One of the objectives of this work is to demonstrate joint state and parameter estimation in the presence of physical state constraints. For the purpose of this study, we will assume uncertainty in the HEX pipe length while other parameters are assumed to be known. To simplify the notation, we denote the right side discretized model in (4) as

$$\boldsymbol{x}_{k+1} = \boldsymbol{f}_k(\boldsymbol{x}_k, L), \tag{5}$$

where $\boldsymbol{u}(t)$ and $\boldsymbol{\phi}$ have been conveniently absorbed in the definition of $\boldsymbol{f}_k(\cdot)$. Only the pipe length L, which is the parameter of interest, has been written explicitly in the argument.

The integral in (4) must be calculated numerically because the equations are nonlinear and high-dimensional. Since the system is numerically stiff, the stiff solver `QNDF` is used to integrate the model (5) forward in time. The model (5) is modified by adding a disturbance term to make it amenable in a general Kalman formulation

$$\boldsymbol{x}_{k+1} = \boldsymbol{f}_k(\boldsymbol{x}_k, L) + \boldsymbol{w}_k, \quad \boldsymbol{w}_k \sim \mathcal{N}(\boldsymbol{0}, \boldsymbol{Q}_k), \tag{6}$$

where $\boldsymbol{w}_k$ denotes a zero-mean white Gaussian process with covariance $\boldsymbol{Q}_k$ that can account for the modeling errors and other disturbances.

The availability of sensors in common vapor compression equipment is limited to measurements of pressure and temperature at a subset of locations in the cycle due to cost and reliability concerns. We assume that the available sensors measure the following vector of temperatures and pressure

$$\boldsymbol{y} \triangleq \left[P_1 \ \theta_2 \ \theta_4 \ \theta_6 \ P_8 \ \theta_8\right]^\top. \tag{7}$$

Therefore, the sensor measurements at t_k denoted by $\boldsymbol{y}_k \triangleq \boldsymbol{y}(t_k)$ can be represented using the following model

$$\boldsymbol{y}_k = \boldsymbol{H}\boldsymbol{x}_k + \boldsymbol{\eta}_k, \quad \boldsymbol{\eta}_k \sim \mathcal{N}(\boldsymbol{0}, \boldsymbol{R}_k), \tag{8}$$

where $\boldsymbol{H} \in \mathbb{R}^{6\times 24}$ is the measurement matrix whose rows are appropriately selected Cartesian basis vectors in $\mathbb{R}^{24}$, and $\boldsymbol{\eta}_k$ is a zero-mean white Gaussian process with covariance $\boldsymbol{R}_k$.

3. SMOOTHING WITH PARTIALLY-KNOWN CONSTRAINTS

As many performance monitoring, analysis and data-driven modeling frameworks are designed to operate on data collected over finite time horizons, the fixed-interval aspect of these applications enables the use of smoothing methods which assimilate sensor measurements obtained within a time interval to estimate states everywhere within that interval and avoid the limitations of filtering algorithms yielding better state-estimation accuracy.

Among several fixed-interval smoothing methods available in the literature, the Rauch-Tung-Striebel (RTS) smoother-type approaches are preferred for many applications as they completely circumvent the need for model inversion, which can be challenging in many circumstances and practically impossible for numerically ill-conditioned systems like vapor compression cycles. RTS-type fixed-interval smoothing methods typically consist of two stages or more commonly referred to as *passes*, namely, a forward pass in time which assimilates data using a filter followed by a backward pass in time which uses state estimates at the future time steps to correct estimates in the past. Equations for these classical methods are readily available, e.g., Crassidis and Junkins (2011). While such methods are optimal for linear systems, they are also widely applied to nonlinear systems using the extended Kalman estimation framework through the use of model linearization.

We present a smoothing method formulated in extended Kalman framework that comprises three passes and incorporates the linear inequality and partially-known nonlinear equality state constraints dictated by the physics of the model, which are often essential to the correct execution of the nonlinear model. We first discuss the state constraints, which are fundamental to the physical system. This is followed by the development of the proposed smoother which is outlined in Algorithm 1.

3.1 State Constraints

Physics-based models of multiphysical systems must enforce constraints on model states and parameters to ensure that the model predictions or outputs satisfy fundamental physical laws. One such constraint relevant to the vapor compression cycle under consideration is the pressure gradient imposed by a given direction of refrigerant flow in the system. With respect to Fig. 1 and state vector (3), the pressure gradient can be expressed as the following inequalities

$$P_1 \geq P_2 \geq \cdots \geq P_7 \geq P_8. \tag{9}$$

The pressure gradient constraint (9) at a time instant t_k can be written in terms of the state as the following vector inequality interpreted element-wise,

$$\boldsymbol{A}\boldsymbol{x}_k \leq 0, \tag{10}$$

where $\boldsymbol{A} \in \mathbb{R}^{7\times 24}$ is an appropriately defined matrix whose most entries are zero, and the nonzero entries are ± 1. The pressure gradient constraint (10) must be satisfied at all time steps within the smoothing interval $k = 1, 2, \cdots, N$.

Another physical constraint that is expected to be satisfied by the cycle states can be specified in terms of total refrigerant mass in the system. In particular, total refrigerant

mass, also referred to as *refrigerant charge*, must be constant over time. In the context of cycle models described in Section 2, the refrigerant charge can be calculated from the state vector as

$$m^* = m_k = g(\boldsymbol{x}_k, L), \quad k = 1, 2, \cdots N. \tag{11}$$

where m^* is the constant but typically unknown total refrigerant mass in the system. The nonlinear map $g(\cdot)$ is known and depends on other known system parameters $\boldsymbol{\phi}$ which have been omitted from (11) for notational simplicity.

The computation of total refrigerant mass by evaluation of nonlinear function $g(\cdot)$ entails computations of refrigerant mass in each HEX finite volume and summing them up. Refrigerant mass in each HEX finite control volume is determined by the product of physical volumes and the respective refrigerant densities calculated using known thermodynamic states, i.e. pressure and specific enthalpy, and the refrigerant's thermodynamic equation of state.

Contrary to (11), it should be noted that the total refrigerant mass in a real-world vapor compression system does not remain constant as the refrigerant often leaks from the system over time. However, the associated time-constant for this process can be of an order of several months to a few years. Therefore, the total refrigerant mass can be assumed to be constant over relatively shorter time horizons as the real-world data available from such systems is typically collected over few days and made available for processing.

Equations (10) and (11) represent state constraints that must be satisfied at all time steps. Although simulation models (2) of the cycle generally satisfy such physical constraints, the state estimates obtained from a standard estimation method may not necessarily satisfy these constraints. These errors can lead to violations of physical laws and failure of computational models, which are often designed under the assumption that they operate in valid regions where such constraints are satisfied. Therefore, state constraints represented by (10) and (11) must be explicitly incorporated into the estimation process.

Extended and ensemble Kalman smoothing methods incorporating only the pressure constraint (10) for state estimation of vapor compression cycles were recently presented by Deshpande et al. (2022). Linear inequality constraints (10) were enforced using truncation of probability density function (PDF) in the extended Kalman framework and we will adopt a similar strategy in the present work.

In comparison, charge constraints (11) are more difficult to incorporate into the estimation process because the actual refrigerant mass m^* in a system is typically not known with a high degree of precision. The uncertainty around the refrigerant mass in a deployed system stems from many different factors including unit-to-unit manufacturing variability, refrigerant leakage from the system over time, and refrigerant replenishment during maintenance events. While there are a variety of methods to estimate changes in the mass for vapor-compression cycles, the more general problem of directly estimating the total mass is an open research problem in the field. In this work, we thus present a novel approach for computation of refrigerant mass via state and parameter estimation of the vapor compression system.

Since the total refrigerant mass is unknown and must be estimated, mechanisms for enforcing (11) during estimation are not straightforward. However, (11) still represents important information about the system that could be beneficial for state estimation. In particular, as per (11), high-dimensional state vector $\boldsymbol{x}$ admits a low-dimensional representation and resides on a partially-known (since m^* is unknown) manifold constrained by the nonlinear map $g(\cdot)$. We incorporate this constraint, hereafter referred to as the *manifold constraint* to distinguish it from the pressure constraint (10), in the smoothing context wherein estimated charge can be used for a posteriori analysis to improve state estimation accuracy. Data-driven modeling efforts for vapor compression cycles could significantly benefit from the improved smoothing accuracy as observed by Chinchilla et al. (2022).

The proposed multi-pass smoother incorporating (10) and (11) for a given measurement dataset is outlined in Algorithm 1 and summarized below. It comprises of three passes which will be discussed in detail in the remainder of this section.

(1) First pass (forward in time): Filtering equations enforce pressure constraint (10) to estimate unknown parameters and refrigerant mass,
(2) Second pass (forward in time): Filtering equations incorporate both pressure constraint (10) and charge manifold constraint (11) using the estimated refrigerant mass to estimate states, and
(3) Third pass (backward in time): Smoothing pass incorporating pressure constraint (10) to refine state estimates.

Algorithm 1 MC-EKS

Data: $\boldsymbol{y}_k$, $k = 1, 2, \cdots, N$
Initialize: $\boldsymbol{x}_1^-$, $\boldsymbol{P}_1^-$
for $k = 1, 2, \cdots, N$ **do**
  Execute filtering steps (14) *// First pass*
end for
Compute $\hat{L}$, $\hat{m}$ from converged estimates and set Z_k.
for $k = 1, 2, \cdots, N$ **do**
  Sample $m_k \sim \mathcal{N}(\hat{m}, Z_k)$
  $\tilde{\boldsymbol{y}}_k \leftarrow \begin{bmatrix} \boldsymbol{y}_k^\top & m_k \end{bmatrix}^\top$
  Execute filtering steps (19) *// Second pass*
end for
$\hat{\boldsymbol{P}}_N \leftarrow \boldsymbol{P}_N^+$, $\hat{\boldsymbol{x}}_k \leftarrow \boldsymbol{x}_k^+$
for $k = N, N-1, \cdots, 1$ **do**
  Execute smoothing steps (22) *// Third pass*
end for

3.2 State and Parameter Estimation

We present an extended Kalman filter for joint state and parameter estimation incorporating pressure constraints (10) in this subsection. As discussed in the previous section, the equations below are explicitly developed for the present case in which the HEX pipe length is the only parameter of interest for the scope of this study. However, this method can be readily extended to more

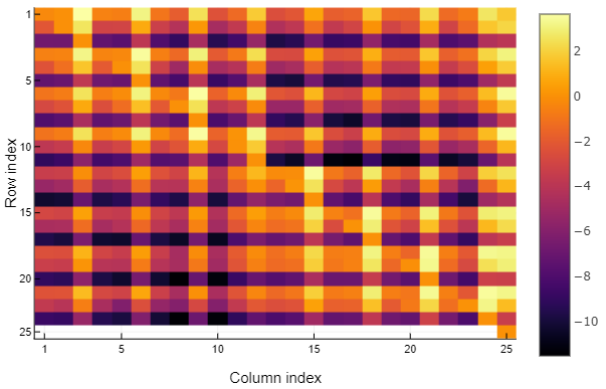

Fig. 2. Structure of the augmented Jacobian matrix. Heatmap shows absolute values of the nonzero elements of $\tilde{\boldsymbol{F}}_k$ on the log-scale.

general settings to estimate another parameter or set of parameters.

We augment the models (6) and (8) to facilitate pipe length estimation as follows.

$$\begin{aligned} \tilde{\boldsymbol{x}}_{k+1} &= \tilde{\boldsymbol{f}}_k(\tilde{\boldsymbol{x}}_k) + \tilde{\boldsymbol{w}}_k \\ \boldsymbol{y}_k &= \tilde{\boldsymbol{H}}\tilde{\boldsymbol{x}}_k + \boldsymbol{\eta}_k \end{aligned} \tag{12}$$

where

$$\tilde{\boldsymbol{x}}_k \triangleq \begin{bmatrix} \boldsymbol{x}_k \\ L_k \end{bmatrix}, \ \tilde{\boldsymbol{f}}_k \triangleq \begin{bmatrix} \boldsymbol{f}_k(\boldsymbol{x}_k, L_k) \\ L_k \end{bmatrix}, \ \tilde{\boldsymbol{w}}_k \triangleq \begin{bmatrix} \boldsymbol{w}_k \\ v_k \end{bmatrix}, \tag{13}$$

$\tilde{\boldsymbol{H}} \triangleq [\boldsymbol{H} \ \boldsymbol{0}]$, $v_k \sim \mathcal{N}(\boldsymbol{0}, V_k)$ and V_k is typically set to a small value, $\tilde{\boldsymbol{w}}_k \sim \mathcal{N}(\boldsymbol{0}, \tilde{\boldsymbol{Q}}_k)$, and $\tilde{\boldsymbol{Q}}_k$ is a block-diagonal matrix with components $\boldsymbol{Q}_k$ and V_k.

The constrained extended Kalman filtering equations for the augmented model (12) are given as follows:

Measurement update:

$$\tilde{\boldsymbol{K}}_k = (\tilde{\boldsymbol{P}}_k^- \tilde{\boldsymbol{H}}_k^\top)(\tilde{\boldsymbol{H}}_k \tilde{\boldsymbol{P}}_k^- \tilde{\boldsymbol{H}}_k^\top + \boldsymbol{R}_k)^{-1} \tag{14a}$$

$$\tilde{\boldsymbol{P}}_k^+ = (\boldsymbol{I} - \tilde{\boldsymbol{K}}_k \tilde{\boldsymbol{H}}_k)\tilde{\boldsymbol{P}}_k^- \tag{14b}$$

$$\tilde{\boldsymbol{x}}_k^+ = \tilde{\boldsymbol{x}}_k^- + \tilde{\boldsymbol{K}}_k(\boldsymbol{y}_k - \tilde{\boldsymbol{H}}_k \tilde{\boldsymbol{x}}_k^-) \tag{14c}$$

$$\tilde{\boldsymbol{x}}_k^+, \tilde{\boldsymbol{P}}_k^+ \leftarrow \texttt{PDFTrunc}(\tilde{\boldsymbol{x}}_k^+, \tilde{\boldsymbol{P}}_k^+) \tag{14d}$$

Time update:

$$\tilde{\boldsymbol{P}}_{k+1}^- = \tilde{\boldsymbol{F}}_k \tilde{\boldsymbol{P}}_k^+ \tilde{\boldsymbol{F}}_k^\top + \tilde{\boldsymbol{Q}}_k \tag{14e}$$

$$\tilde{\boldsymbol{x}}_{k+1}^- = \tilde{\boldsymbol{f}}_k(\tilde{\boldsymbol{x}}_k^+) \tag{14f}$$

where $\tilde{\boldsymbol{x}}_k^+$ and $\tilde{\boldsymbol{P}}_k^+$ denote a posteriori mean and covariance of the augmented state vector at time t_k obtained after assimilating all sensor measurements up to time step k, whereas the a priori mean and covariance obtained after assimilating all sensor measurements up to time step $k-1$ are denoted by $\tilde{\boldsymbol{x}}_k^-$ and $\tilde{\boldsymbol{P}}_k^-$. Similar notations are followed throughout the paper unless specified otherwise. The Jacobian of the augmented system at $\tilde{\boldsymbol{x}}_k^+$ is denoted by $\tilde{\boldsymbol{F}}_k$, i.e.,

$$\tilde{\boldsymbol{F}}_k \triangleq \frac{\partial \tilde{\boldsymbol{f}}_k}{\partial \tilde{\boldsymbol{x}}}(\tilde{\boldsymbol{x}}_k^+) = \begin{bmatrix} \dfrac{\partial \boldsymbol{f}_k}{\partial \boldsymbol{x}}(\boldsymbol{x}_k^+, L_k^+) & \dfrac{\partial \boldsymbol{f}_k}{\partial L}(\boldsymbol{x}_k^+, L_k^+) \\ \boldsymbol{0}_{1\times 24} & 1 \end{bmatrix}. \tag{15}$$

The structure of $\tilde{\boldsymbol{F}}_k$ is illustrated in Fig. 2 via a heatmap which shows absolute values of the nonzero elements of $\tilde{\boldsymbol{F}}_k$ on the log-scale in a normalized coordinate system. $\tilde{\boldsymbol{F}}_k$ is typically a dense matrix with no particular structure since it is Jacobian of the discretized system (4) involving numerical integration of continuous-time dynamics.

Remark 1. Computation of Jacobian is challenging because $\boldsymbol{f}_k(\cdot)$ involves an integral in (4) which is computed numerically using stiff solvers. AD-compatibility of the cycle model discussed in Section 2 and the solver `QNDF` allows an efficient computation of Jacobian matrices.

The measurement update in (14) is modified to account for the pressure constraints. The function `PDFTrunc` in (14d), returns the corrected posterior mean and covariance that satisfy the state constraints if the posterior mean obtained from standard Kalman update equations violate the pressure constraint (10).

We adopt the PDF truncation approach discussed in Simon and Simon (2010) to enforce constraints on posterior mean and covariance because it incorporates constraint information in both mean and covariance matrix, whereas other approaches that project the estimate on the constraint set only enforce the constraints on the mean without correcting the error covariance matrix. It is expected that the uncertainty in the state estimate represented by the error covariance will decrease since the system state must satisfy known constraints.

The PDF truncation method sequentially applies an appropriate coordinate transformation that leverages Gram-Schmidt orthonormalization such that only boundedness constraint are to be imposed on a scalar variable at a time. The scalar Gaussian PDF is truncated at the boundaries of the linear constraints by setting the density outside the feasible region to zero. The resulting truncated PDF is then normalized to have the total probability of unity within the feasible bounds. While the detailed equations for this method are available in Simon and Simon (2010), the function $\texttt{PDFTrunc}(\boldsymbol{x}, \boldsymbol{P})$ essentially returns $\boldsymbol{x}$ and $\boldsymbol{P}$ if the constraint is pressure constraint (10) is satisfied, and truncates the PDF and returns the constrained version of $\boldsymbol{x}$ and $\boldsymbol{P}$ if not.

3.3 State Filtering Leveraging Estimated Parameters

Let us assume that the augmented filter (14) is allowed to run over a sufficiently long time interval so that the estimates of the unknown parameters converge to certain values, for instance, see Fig. 3. In this scenario, the pipe length and state vector from the converged estimates of augmented filter (14) can be used to estimate total refrigerant mass using known map (11). If $\hat{L}$ and $\hat{m}$ denote these estimated parameters from (14) at the end of the time-interval, for example at $t = 100$ s in Fig. 3, we may investigate whether these refined parameter estimates can be used to improve state estimates at earlier time-steps in an a posteriori analysis. We thus present such an approach to incorporate estimated refrigerant mass along with manifold constraint (11) in state estimation in this subsection.

We incorporate (11) in the Kalman filtering framework via synthetic or simulated measurements of the refrigerant mass. In particular, we define a synthetic sensor measurement as follows

$$m_k = g(\boldsymbol{x}_k, \hat{L}) + z_k \tag{16}$$

where $z_k \sim \mathcal{N}(\mathbf{0}, Z_k)$, and the synthetic sensor measurements m_k are actually sampled from the distribution $\mathcal{N}(\hat{m}, Z_k)$, where Z_k can be assigned a smaller value for a stricter enforcement of the constraint (11). Since $\hat{m}$ is an error-prone estimate, a suitable value for Z_k could also be calculated from the posterior error covariance of the converged estimates of augmented filter (14). An augmented measurement model immediately follows from (8), (16)

$$\tilde{\boldsymbol{y}}_k = \tilde{\boldsymbol{g}}(\boldsymbol{x}_k) + \tilde{\boldsymbol{\eta}}_k \tag{17}$$

where

$$\tilde{\boldsymbol{y}}_k \triangleq \begin{bmatrix} \boldsymbol{y}_k \\ m_k \end{bmatrix}, \ \tilde{\boldsymbol{g}}(\boldsymbol{x}_k) \triangleq \begin{bmatrix} \boldsymbol{H}\boldsymbol{x}_k \\ g(\boldsymbol{x}_k, \hat{L}) \end{bmatrix}, \ \tilde{\boldsymbol{\eta}}_k \triangleq \begin{bmatrix} \boldsymbol{\eta}_k \\ z_k \end{bmatrix}, \tag{18}$$

$\tilde{\boldsymbol{\eta}}_k \sim \mathcal{N}(\mathbf{0}, \tilde{\boldsymbol{R}}_k)$, and $\tilde{\boldsymbol{R}}_k$ is a block-diagonal matrix with components $\boldsymbol{R}_k$ and Z_k.

An extended Kalman filter that incorporates pressure constraint (10) and utilizes (16) for enforcing manifold constraint (11) is given as follows:

Measurement update:

$$\boldsymbol{K}_k = (\boldsymbol{P}_k^- \tilde{\boldsymbol{G}}_k^\top)(\tilde{\boldsymbol{G}}_k \boldsymbol{P}_k^- \tilde{\boldsymbol{G}}_k^\top + \tilde{\boldsymbol{R}}_k)^{-1} \tag{19a}$$

$$\boldsymbol{P}_k^+ = (\boldsymbol{I} - \boldsymbol{K}_k \tilde{\boldsymbol{G}}_k)\boldsymbol{P}_k^- \tag{19b}$$

$$\boldsymbol{x}_k^+ = \boldsymbol{x}_k^- + \boldsymbol{K}_k(\tilde{\boldsymbol{y}}_k - \tilde{\boldsymbol{g}}(\boldsymbol{x}_k^-)) \tag{19c}$$

$$\boldsymbol{x}_k^+, \boldsymbol{P}_k^+ \leftarrow \texttt{PDFTrunc}(\boldsymbol{x}_k^+, \boldsymbol{P}_k^+) \tag{19d}$$

Time update:

$$\boldsymbol{P}_{k+1}^- = \boldsymbol{F}_k \boldsymbol{P}_k^+ \boldsymbol{F}_k^\top + \boldsymbol{Q}_k \tag{19e}$$

$$\boldsymbol{x}_{k+1}^- = \boldsymbol{f}_k(\boldsymbol{x}_k^+, \hat{L}) \tag{19f}$$

where $\tilde{\boldsymbol{G}}_k$ is the Jacobian of augmented measurement model (17) at $\boldsymbol{x}_k^-$, i.e.,

$$\tilde{\boldsymbol{G}}_k \triangleq \frac{\partial \tilde{\boldsymbol{g}}_k}{\partial \boldsymbol{x}}(\boldsymbol{x}_k^-) = \begin{bmatrix} \boldsymbol{H} \\ \dfrac{\partial g_k}{\partial \boldsymbol{x}}(\boldsymbol{x}_k^-, \hat{L}) \end{bmatrix}. \tag{20}$$

and $\boldsymbol{F}_k$ is the Jacobian of $\boldsymbol{f}_k$ at $\boldsymbol{x}_k^+$, i.e.,

$$\boldsymbol{F}_k \triangleq \frac{\partial \boldsymbol{f}_k}{\partial \boldsymbol{x}}(\boldsymbol{x}_k^+, \hat{L}), \tag{21}$$

while (19d) enforces the pressure constraints.

Remark 2. Although the data assimilation equations (19) represent a forward pass in time, they actually constitute a *smoothing* operation when used with the same sensor data set used in (14) because (19) uses the converged parameter estimates at future time step $k = N$ to improve state estimates in the past at $k \leq N-1$. However, (19) can also be used in a true filtering sense at time-steps $k \geq N+1$ once parameters are estimated at $k = N$.

The equations for the final smoothing pass are presented next.

3.4 Refining State Estimates by Smoothing

Let $\{\boldsymbol{x}_k^-, \boldsymbol{P}_k^-\}$ and $\{\boldsymbol{x}_k^+, \boldsymbol{P}_k^+\}$ be the prior and posterior mean-covariance pairs obtained from the filtering pass (19), respectively. The constrained extended Kalman smoother that computes smoothing posteriors $\{\hat{\boldsymbol{x}}_k, \hat{\boldsymbol{P}}_k\}$ at time steps k is given as follows:

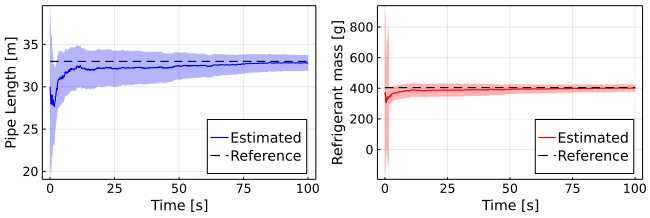

Fig. 3. Solid lines show estimated pipe length (left) and refrigerant mass (right) while shaded areas show 3σ bounds. Dashed lines show reference parameter values $L^* = 33$ m and $m^* = 404.7$ g.

$$\boldsymbol{S}_k = \boldsymbol{P}_k^+ \boldsymbol{F}_k^\top \left(\boldsymbol{P}_{k+1}^-\right)^{-1} \tag{22a}$$

$$\hat{\boldsymbol{P}}_k = \boldsymbol{P}_k^+ - \boldsymbol{S}_k \left(\boldsymbol{P}_{k+1}^- - \hat{\boldsymbol{P}}_{k+1}\right) \boldsymbol{S}_k^\top \tag{22b}$$

$$\hat{\boldsymbol{x}}_k = \boldsymbol{x}_k^+ + \boldsymbol{S}_k \left(\hat{\boldsymbol{x}}_{k+1} - \boldsymbol{x}_{k+1}^-\right) \tag{22c}$$

$$\hat{\boldsymbol{x}}_k, \hat{\boldsymbol{P}}_k \leftarrow \texttt{PDFTrunc}(\hat{\boldsymbol{x}}_k \hat{\boldsymbol{P}}_k) \tag{22d}$$

The equations above, except (22d), are the well-known RTS smoother equations, and have been augmented with (22d) to enforce the state constraints. The smoothing process (22) represents a backward pass in time, as it must be started at the end of the smoothing window at $k = N$. The smoother is therefore initialized at $\hat{\boldsymbol{x}}_N = \boldsymbol{x}_N^+$ and $\hat{\boldsymbol{P}}_N = \boldsymbol{P}_N^+$, and the mean and covariance are updated sequentially backwards in time up to the start of the window at $k = 1$.

This proposed multi-pass constrained extended Kalman smoother incorporating both state constraints (9) and the manifold constraint (11) in the estimation process is summarized in Algorithm 1 using equations developed in this section, and abbreviated as MC-EKS.

4. NUMERICAL RESULTS

The numerical simulations are facilitated by a model obtained by discretizing (2) with the time step of 0.1 s. The reference or true pipe length is assumed to be $L^* = 33$ m, which is typical for the vapor compression cycle model described in Section 2. The covariance $\boldsymbol{Q}_k$ in (6) is assumed to be a constant diagonal matrix whose variance entries corresponding to pressure, specific enthalpy and temperature are $7 \cdot 10^6, 6 \cdot 10^5, 2 \cdot 10^{-2}$, respectively. Similarly, noise variances in the measurement model (8) are set to $2.5 \cdot 10^8$ and 10^{-1} respectively for pressure and temperature sensors, while assuming $\boldsymbol{R}_k$ to be a constant diagonal matrix.

The control inputs and system parameters (except the pipe length and refrigerant charge) are assumed to be known during the simulation over a timespan of 100 s. The compressor speed remains constant with time except a single jump at $t = 10$ s from 50 Hz to 55 Hz. Similarly, the outdoor ambient temperature is assumed to change from 305.15 K to 308.15 K at $t = 20$ s, while the expansion valve position makes a jump at $t = 40$ s from 56.4% to 62.4%. The reference model's state is initialized with equal pressures 2.8 MPa and 1 MPa in outdoor and indoor HEX volumes respectively, all pipe wall temperatures are set to 308.15 K, while the specific enthalpy is initialized with linear variation in each HEX from 500 kJ/kg at volumes 1 and 8 to 280 kJ/kg at volumes 4 and 5 in Fig. 1. The

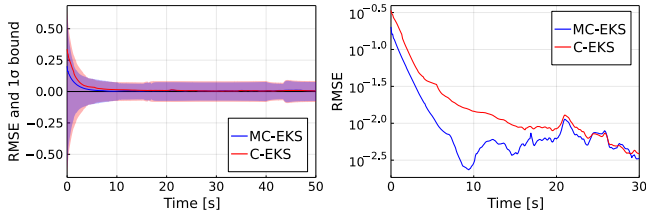

Fig. 4. *Left:* Comparison of RMSE and 1σ bounds for MC-EKS and C-EKS. *Right:* Comparison of RMSE during initial transients. Both RMSE and 1σ are normalized.[2]

sensor measurements to be used in state and parameter estimation are generated by the perturbing the reference model state trajectories using noise values sampled from the corresponding sensor noise distributions.

The results for the filtering pass (14) are discussed first, followed by overall results for Algorithm 1.

4.1 Parameter Estimation

The augmented filter (14) is used to estimate the unknown system parameters along with the states of the cycle. The filtering estimates are initialized as follows. The standard deviations of the initial state estimates are assumed to be 10% of their values of pressure and specific enthalpy, and 1% of temperature of the reference model. The prior mean state estimate is sampled from this distribution and projected on the constraint set (9). The initial prior distribution of the pipe length is assumed to be Gaussian with mean 30 m and standard deviation 3 m. The process variance V_k corresponding with pipe length dynamics is varied from 10^{-2} to 10^{-5} as time progresses. While time-varying V_k is not strictly necessary, doing so often yields a better trade-off between consistency and convergence of the estimate.

Fig. 3 shows the parameter estimates and the corresponding 3σ bounds obtained using the filtering equations (14), which constitute the first pass of Algorithm 1. The refrigerant mass is estimated using the augmented filter's posterior state estimate and the known map $g(\cdot)$ in (11), and its variance is estimated using first-order Taylor series expansion of $g(\cdot)$ similar to extended Kalman time-update equations. As seen from Fig. 3, both estimated pipe length and refrigerant mass eventually converge to the reference values. At the end of 100 s in Fig. 3, the pipe length and refrigerant mass have estimated values of $\hat{L} = 32.86$ m and $\hat{m} = 401.8$ g, indicating an accuracy of better than 99%. These results show the efficacy of joint state and parameter estimation using augmented filter (14), and more importantly, the efficiency of cycle-level data-assimilation paradigm for accurate estimation of unknown refrigerant mass in the system.

4.2 State Estimation

Estimated parameters from (14), i.e., $\hat{L} = 32.86$ m and $\hat{m} = 401.8$ g, are then used for further refining state estimates using (19) and (22) which constitute the remaining two passes of Algorithm 1. The synthetic measurements for the refrigerant mass are sampled from $m_k \sim \mathcal{N}(\hat{m}, Z_k)$,

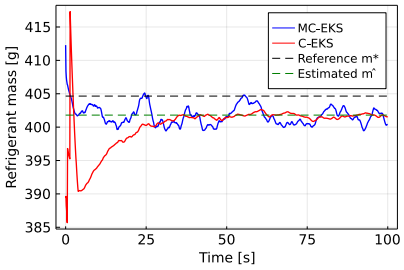

Fig. 5. Refrigerant mass back-calculated from MC-EKS and C-EKS state estimates.

where $Z_k = 6.3 \cdot 10^{-5}$ is a constant whose value is equal to the variance of estimated refrigerant mass at $t = 100$ s in Fig. 3.

Fig. 4 shows the state-estimation accuracy in terms of RMSE and the square-root of trace of error covariance matrix, i.e. 1σ bound, which both have been normalized.[2] The performance of the proposed MC-EKS approach which incorporates manifold constraint (11) via synthetic measurements in addition to the pressure constraints (9), is compared with C-EKS algorithm which only enforces the pressure constraints (9) without utilizing additional information about the system represented by the charge constraint (11). C-EKS follows steps similar to Algorithm 1 with comparable computational cost, except the original sensor measurements (8) are used during the second filtering pass instead of augmented synthetic sensor measurements (17).

As seen from Fig. 4, the MC-EKS method demonstrates smaller estimation RMSE as it utilizes the additional information represented by charge manifold (11), whereas C-EKS completely disregards such information about the system. Trace of the error covariance matrix quantified by 1σ bound in Fig. 4 are comparable for MC-EKS and C-EKS, however, MC-EKS demonstrates a somewhat smaller trace. The improved estimation accuracy of MC-EKS is especially evident during the initial transients shown in the right plot of Fig. 4, wherein the uncertainty is typically large because the initial state of the system is often unknown. Both MC-EKS and C-EKS demonstrate similar accuracy as time progresses, which is expected because both use the same converged parameter estimates obtained from (14) and are expected to converge to similar regions in state-space. However, improved accuracy of MC-EKS during early transients can be leveraged not only to advance data-driven or surrogate modeling efforts which often rely on accurate state estimates, but also to examine other system performance parameters, including the heating/cooling capacity delivered to a space.

Fig. 5 shows the refrigerant mass back-calculated from the state estimates obtained from MC-EKS and C-EKS. Larger deviations of refrigerant mass obtained by C-EKS from the reference value during initial transient is an artifact of the larger associated state-estimation error seen in Fig. 4. On the other hand, MC-EKS demonstrates

[2] Algorithms are implemented in a normalized coordinate system such that all state variable have comparable magnitudes of an order 10^0 at a nominal point to mitigate some effects of the ill-conditioned system dynamics. RMSE and trace are also calculated in this normalized coordinate system.

relatively smaller deviation from the reference value as it incorporates the charge constraint (11) and satisfies it to a better degree than C-EKS, thus, yielding better state-estimation accuracy as seen from Fig. 4. Refrigerant mass obtained from MC-EKS can be seen to oscillate roughly about the estimated charge $\hat{m}$, because the synthetic measurements are generated from a Gaussian with $\hat{m}$ as the mean. Variance of these oscillations can be reduced by decreasing noise variance Z_k in (16). Smaller values of Z_k will enforce the charge manifold constraint more strictly, and will therefore yield even smaller estimation RMSE if such a high-confidence (small Z_k) estimate of m^* is available.

5. CONCLUSION

In this paper, we developed a fixed-interval extended Kalman smoother that incorporates physical constraints during the joint state and parameter estimation of vapor compression cycles. While certain inequality constraints were strictly enforced to ensure that the computational model functions correctly, partially-known equality constraints were incorporated via simulated synthetic measurements to further improve the state estimation accuracy of the smoother. While computations of Jacobian needed for the implementation of the smoother were facilitated by automatic differentiation capability of cycle models, they may still pose computational challenges for large-scale systems for which the proposed smoother can be potentially adapted using Monte Carlo simulation methodologies. Next steps for this work also include the extension of these methods to higher fidelity models that use moist air in multiple heat exchangers, and the performance benchmarking using real-world datasets.

REFERENCES

Bortoff, S. and Laughman, C.R. (2022). Estimation: A key technology for digital twins. In *MERL Technical Reports*. URL `https://www.merl.com/publications/TR2022-127`.

Bortoff, S., Schwerdtner, P., Danielson, C., and Di Cairano, S. (2019). H-infinity loop-shaped model predictive control with heat pump application. In *18th European Control Conference*, 2386–2393.

Cheng, T., He, X.D., and Asada, H. (2005). Nonlinear observer design and experimental verification for heat exchangers during the start-up process. In *2005 American Control Conference*. doi:10.1109/ACC.2005.1470757.

Chinchilla, R., Deshpande, V.M., Chakrabarty, A., and Laughman, C.R. (2022). Learning residual dynamics of vapor compression cycles via physics-augmented neural networks. In *Submitted to 2023 American Control Conference*.

Crassidis, J.L. and Junkins, J.L. (2011). *Optimal Estimation of Dynamic Systems*. Chapman and Hall/CRC.

Deshpande, V.M., Laughman, C.R., Ma, Y., and Rackauckas, C. (2022). Constrained smoothers for state estimation of vapor compression cycles. In *2022 American Control Conference*, 2333–2340.

Ghousein, M. and Witrant, E. (2019). A boundary observer for two phase heat exchangers. In *18th European Control Conference*, 2332–2337. Napoli, Italy.

IEA (2018). The future of cooling. Technical report, International Energy Agency, Paris. URL `https://www.iea.org/reports/the-future-of-cooling`.

Krupa, P., Danielson, C., Laughman, C., Bortoff, S., Burns, D., Di Cairano, S., and Limon, D. (2019). Modelica implementation of centralized MPC controller for a multi-zone heat pump. In *18th European Control Conference*, 1784–1789. doi:10.23919/ECC.2019.8795616.

Laughman, C. and Qiao, H. (2021). Patch-based thermodynamic property models for the subcritical region. In *International Refrigeration and Air-Conditioning Conference at Purdue*, 1–10. Paper 2258.

Ma, Y., Gowda, S., Anantharaman, R., Laughman, C.R., Shah, V., and Rackauckas, C. (2021). ModelingToolkit: A composable graph transformation system for equation-based modeling.

Pantelides, C.C. (1988). The consistent initialization of differential-algebraic systems. *SIAM Journal on Scientific and Statistical Computing*, 9(2), 213–231.

Qiao, H., Aute, V., and Radermacher, R. (2015). Transient modeling of a flash tank vapor injection heat pump system–Part I: Model development. *International Journal of Refrigeration*, 49, 169–182.

Simon, D. and Simon, D.L. (2010). Constrained Kalman filtering via density function truncation for turbofan engine health estimation. *International Journal of Systems Science*, 41(2), 159–171.

Vering, C., Borges, S., Coakley, D., Kruetzfeldt, H., Mehrfeld, P., and Müller, D. (2021). Digital twin design with on-line calibration for HVAC systems in buildings. In *Proceedings of Building Simulation 2021: 17th Conference of IBPSA*, volume 17 of *Building Simulation*, 2938–2945. IBPSA, Bruges, Belgium.